Snap-Through Buckling Reliability Analysis Under Spatiotemporal Variability and Epistemic Uncertainty

Harshini Devathi,* Zhen Hu,† and Sankaran Mahadevan‡
Vanderbilt University, Nashville, Tennessee 37235

DOI: 10.2514/1.J054920

Surrogate models often provide an effective tradeoff between accuracy and efficiency during reliability analysis with expensive physics models. In snap-through buckling reliability analysis, a surrogate model could be built for the critical buckling load, as a function of loading, material properties, geometry, and boundary conditions. However, in the presence of spatiotemporal variability, the response surface of the critical buckling load is often highly nonlinear and irregular, thus rendering commonly used response surface-type surrogate modeling strategies ineffective. This paper proposes a new buckling reliability analysis method based on support vector machines for structures subjected to spatiotemporal variability and in the presence of epistemic uncertainty regarding model inputs and parameters. Bayesian calibration is first used to quantify the epistemic uncertainty in the modeling of spatiotemporal variability under limited data. Upon the modeling of spatiotemporal variability and epistemic uncertainty, a time-dependent reliability analysis method is developed for the snap-through buckling failure by constructing a nonlinear support vector machine classifier. Considering that the computer simulation is computationally expensive and the support vector machine classifier may not be well trained due to limited computational resources, a method is also developed to quantify the uncertainty in the reliability estimate due to classification uncertainty. A curved beam with an uncertain boundary condition, spatially varying cross-section geometry, and spatiotemporally varying loading is used to demonstrate the effectiveness of the proposed method.

I. Introduction

SNAP-THROUGH buckling is an important failure mode of concern during the analysis and design of supersonic/hypersonic vehicle panels under extreme load and temperature conditions [1,2]. Hypersonic aircraft are subject to multiphysics loads such as aerodynamic, thermal, and acoustic loads [3]. This results in a coupled, nonlinear interaction with the structure that could, under extreme conditions, fail through one of the several different failure modes possible (e.g., snap-through, flutter, and thermal fatigue). The current paper focuses on methods to estimate snap-through buckling under various sources of uncertainty.

A system is said to have snapped through if it changes from one stable configuration to another stable configuration [4]. Snap-through buckling is of two kinds (as shown in Fig. 1): postbuckled snap-through and limit-point buckling [5]. In postbuckled snap-through, after the system has buckled, it would snap from one stable configuration to another in the presence of perturbations [6]. Limit-point buckling corresponds to the stiffness of the structure decreasing to zero as the load is increased and the structure snaps through to a high-deflection stable limit state [6]. Among the these two types of snap-through buckling, limit-point buckling is the focus of this paper since it is important from the point of view of structural design.

Snap-through buckling analysis has been extensively investigated in the literature. For example, Haftka and Mallett [4] derived analytical expressions for the critical buckling load by using Koiter's method. Pi et al. [7] studied the nonlinear dynamic snap-through buckling behavior of shallow arches under suddenly applied long-duration uniform loads. Similarly, analytical expressions for static critical loads for sinusoidal arches under different loading conditions, such as sinusoidally distributed loads, uniformly distributed loads, and point loads, in the presence of flexible boundary conditions have been investigated [7]. Prezkop and Rizzi [8] studied the snap-through behavior of thermally buckled structures using a reduced-order model. Snap-through buckling reliability analysis methods that account for the randomness in the structure geometry, variability in the material property, and uncertainty in the boundary conditions have been studied in recent years. For instance, Alibrandi et al. [9] proposed an efficient procedure for buckling reliability analysis using a response surface method based on rational functions, Papadopoulos and Papadrakakis [10] studied the effect of material and thickness variability on the buckling load of shells with initial imperfections, Van de Lindt and Pei [11] presented a buckling reliability analysis procedure by investigating the effect of the deterioration of steel beam ends on the steel beam buckling capability, and Choi et al. [12] used a polynomial chaos expansion (PCE) surrogate model for the buckling reliability analysis of a joined-wing model. Buckling in the presence of manufacturing imperfections, variable thickness, and initial imperfections has also been carried out in the past by Hilburger et al. [13], Koiter et al. [14], Starnes et al. [15], and Chryssanthopoulos et al. [16].

From the previously mentioned literature review, it is found that most reported buckling reliability analysis studies rely on the computation of the critical buckling load, which is affected by many sources of uncertainty. Besides, current buckling reliability analysis methods are based on assumptions regarding loading, such as uniformly distributed load or concentrated load. In practical situations, however, both material property and loads may have spatial and/or temporal variability. For example, a hypersonic aircraft panel experiences loads varying along its surface and with time throughout the flight mission. The spatiotemporal variability makes the buckling reliability analysis difficult. In addition to that, how to properly represent the spatiotemporal variability also creates a challenge. The reliability analysis also needs to account for sources of epistemic uncertainty due to limited data for the quantification of spatiotemporal variability.

To overcome the previously mentioned shortcomings, this paper proposes a new buckling reliability analysis method that can consider spatiotemporal variability and epistemic uncertainty using support vector machines (SVMs) [17]. SVMs are a powerful classification tool, which can construct highly nonlinear continuous, discontinuous, or disjoint functions between classes in a multidimensional domain. Applications of SVMs in time-independent reliability analysis have been investigated by Basudhar and Missoum [17] by

Received 27 November 2015; revision received 12 May 2016; accepted for publication 21 June 2016; published online 25 August 2016.

*Graduate Student, Department of Civil and Environmental Engineering; harshini.devathi@vanderbilt.edu.

†Postdoctoral Research Scholar, Department of Civil and Environmental Engineering; zhen.hu@vanderbilt.edu.

‡Department of Civil and Environmental Engineering; sankaran.mahadevan@vanderbilt.edu (Corresponding Author).

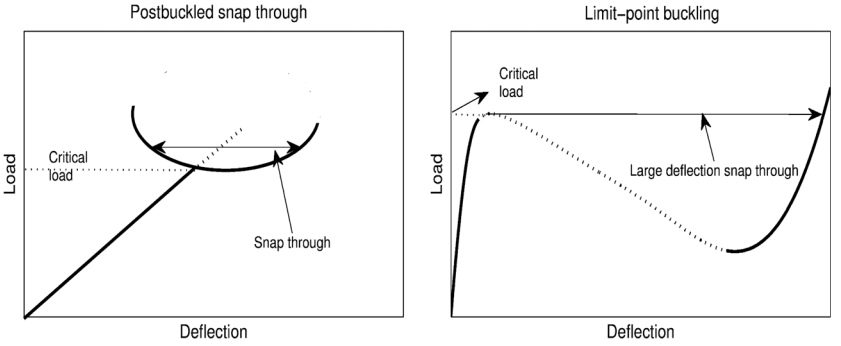

Fig. 1 Two types of snap-through buckling.

constructing failure boundaries using SVMs. Based on that, Basudhar and Missoum [18] employed a probabilistic SVM using sigmoid-based SVM model to account for classification uncertainty. In this paper, a SVM is combined with a spatiotemporal modeling technique [using singular value decomposition (SVD) and the autoregressive moving average (ARMA)] to perform time-dependent buckling reliability analysis under epistemic uncertainty.

The modeling of spatiotemporal variability based on experimental data is investigated first. The epistemic uncertainty in the modeling of spatiotemporal variability due to limited data is quantified using Bayesian calibration [19]. In the presence of spatiotemporal variability, as stated before, the response surface is not amenable to response surface-based surrogate modeling. Therefore, buckling reliability analysis is performed by training a surrogate model for the buckling failure event using SVMs. Since the computer simulation of buckling analysis of a complicated system is usually computationally expensive, the SVM classifier may not be well trained due to limited computational resources. A method is developed in this paper to quantify the uncertainty in the buckling reliability estimate due to the classification uncertainty. This paper develops new methods in three directions: 1) representation of spatiotemporal variability based on experimental data, 2) quantification of the epistemic uncertainty in the modeling of spatiotemporal variability, and 3) buckling reliability analysis under spatiotemporal variability and epistemic uncertainty.

The remainder of the paper is organized as follows. We first provide background concepts on buckling reliability analysis and spatiotemporal variability in Sec. II. Section III presents the proposed methodology. A curved beam with an uncertain boundary condition is used in Sec. IV to demonstrate the proposed method. Section V gives the concluding remarks.

II. Background

A. Snap-Through Buckling

Snap-through buckling is commonly identified by estimating the critical buckling load of the structure using analytical or numerical methods and then comparing it with the actual load value. If the actual load exceeds the critical load, the system has snapped through. The limit state function for buckling failure is defined as

$$g(\boldsymbol{x}) = F - F_{\text{cr}}(\boldsymbol{x}) \tag{1}$$

where F is the actual load, $F_{\text{cr}}(\boldsymbol{x})$ is the critical buckling load, and $\boldsymbol{x}$ is a vector of variables that affect the value of the critical buckling load.

The previous equation indicates that the most critical step for the buckling failure analysis is the computation of the critical buckling load $F_{\text{cr}}(\boldsymbol{x})$. The evaluation of the critical buckling load has been extensively investigated in the literature as described in Sec. I. Among the available methods, a widely used method is the analytical expression derived by Fung and Kaplan [20,21] for a sinusoidal arch in the presence of uniform pressure loading and flexible boundary conditions. Consider a sinusoid shaped beam as shown in Fig. 2, where end 1 of the beam is fully fixed and the other end has a horizontal spring. Here, the motion is allowed only along the x axis and is restrained along the y and z axes. In Fung and Kaplan's method, the critical snap-through buckling load can be estimated by following the procedure given in the following.

1) Estimate the parameters $\upsilon = \frac{\ell}{2}\sqrt{\frac{\Lambda}{I}}$ and $\beta = \frac{K_d}{(K_d + E\Lambda/L)}$, where Λ indicates the cross-sectional area, I indicates the moment of inertia of the cross-sectional area, E is the Young modulus, L is the beam length, ℓ is the rise of the arch, K is the compliance coefficient of the spring, and K is related to the spring stiffness K_d as $K = 500/K_d$. A value of $K = 0$ indicates a completely fixed end, and a value of $K = \infty$ indicates a completely free end.

2) Solve for υ using $(\beta\upsilon^2 - 4) = 4(\beta\upsilon^2 - 1)^3/243$. Let υ_0 be the value of the minimum positive root; then the nondimensional value of the critical load R_{cr} can be estimated as [16,17]

$$R_{\text{cr}} = \begin{cases} \pi\left(\upsilon + \sqrt{4(\beta\upsilon^2 - 1)^3/(27\beta)}\right)/4, & 1/\sqrt{\beta} < \upsilon \le \upsilon_0, \\ \pi\left(\upsilon + 3\sqrt{(\beta\upsilon^2 - 4)/\beta}\right)/4, & \upsilon > \upsilon_0 \end{cases} \tag{2}$$

The critical snap-through buckling load F_{cr} is then estimated as $F_{\text{cr}} = 2\pi^4 EIR_{\text{cr}}/(L^4\sqrt{I/\Lambda})$, where F_{cr} is the pressure load acting per unit width of the structure.

The previous equations are only for a half-sine-shaped beam with the configuration given in Fig. 2. Other methods have also been developed to compute the critical buckling load by using finite-element analysis. For example, Elishakoff et al. [22] developed a nonlinear buckling analysis method using stochastic and non-stochastic convex models, and Haftka and Mallett [4] used Koiter's method to perform snap-through buckling analysis based on finite-element analysis. Based on the available buckling analysis methods, a group of probabilistic buckling analysis methods have been proposed to account for uncertainty sources such as geometry imperfections, material property variability, and random boundary conditions. For example, Kogiso et al. [23] studied the effects of correlation between random variables on the buckling failure of a composite plate, and Elishakoff et al. [24] investigated buckling reliability analysis with random imperfections using the first-order second-moment analysis method.

Even though it may be possible to estimate the critical buckling loads using analytical expressions or finite-element simulations, obtaining a specific solution for the critical load can be tedious for some problems involving spatial variation of the load or the material properties. This issue is discussed in Sec. III.B.

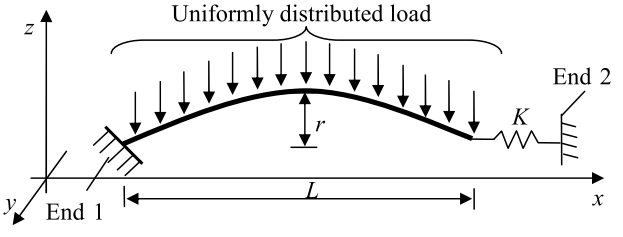

Fig. 2 Curved beam with flexible boundary condition at End 2.

B. Spatiotemporal Variability and Epistemic Uncertainty

In many practical systems, several physical quantities vary both spatially and temporally. For example, the loads acting on the body of an aircraft, hull of a ship, etc., vary both over space and time. Hypersonic vehicle panels are subjected to large thermal and aerodynamic stresses varying over space and time. In such extreme environments, small variations in physical quantities can give rise to large fluctuations in stress, thus strongly affecting the failure probability.

In the current work, we consider the reliability analysis for snap-through buckling in the presence of both spatial and temporal variability. In snap-through buckling, a system or a curved structure snaps from one stable configuration to another. Snap-through deformation can be either of small amplitude or large amplitude. Irrespective of the magnitude of the deformation, the presence of small disturbances can cause snap through in an otherwise stable system. Large-amplitude snap-through is, especially, more sensitive to such fluctuations.

Figure 3 shows a snapshot of a spatiotemporally varying random field. The horizontal coordinate refers to space, and the vertical coordinate refers to time. A horizontal slice shows the variation of the load over space, at a particular time instant. Similarly, a vertical slice gives the variation of the load over time at a particular spatial location. In snap-through buckling reliability analysis with the spatiotemporal variability, there are mainly two challenges, which are 1) how to represent and quantify the spatiotemporal variability based on available history or experimental data and 2) how to predict the reliability based on the modeling of spatiotemporal variability. The first challenge comes from the lack of analytical expressions for spatiotemporal variability. The second challenge stems from the fact that when we have spatiotemporal variation the response surface is irregular and hence cannot be modelled using commonly used numerical surrogate modelling techniques (discussed in Sec. III.B). In addition, the data available to model the spatiotemporal variability may be limited. It may be typical for the designer to have just one set of data obtained at a few locations over different time instants but no more than that. In that case, the parameters of the spatiotemporal field may not be known accurately. This is epistemic uncertainty (lack of knowledge), on top of aleatory uncertainty (natural variability over space and time).

In the following section, we will first discuss how to represent the spatiotemporal variability and then investigate how to quantify the epistemic uncertainty in the model of spatiotemporal variability. Based on that, we develop the buckling reliability analysis method.

III. Proposed Methodology

A. Representation of Spatiotemporal Variability Based on Data

In this paper, the spatiotemporal variability is modeled as a stationary random field. A stationary random field $x(s,t)$ can be decomposed into a mean term $\mu(s)$ and the variation term $z(s,t)$. Based on the decomposition, the random field is represented as

$$x(s,t) = \mu(s) + \sum_{i=1}^{r} w_i(t)\vartheta_i(s) \tag{3}$$

where s is the spatial coordinate, t is the temporal coordinate, $\vartheta_i(s)$ is the ith important feature used to model the variation, r is the number of importance features, and $w_i(t)$ is used to represent the variation over snapshots.

A critical step in the modeling of the random field using the previous equation is to determine the important features $\vartheta_i(s)$, $i = 1, 2, \cdots, r$. During the past decades, a group of methods has been proposed to model a random field, such as the midpoint method [25], the spatial averaging method [25], proper orthogonal decomposition (POD) [26,27], etc. The POD method, which is also called principal component analysis or Karhunen–Loeve decomposition, solves an optimization model to determine the important features [28],

$$\max f_{\text{obj}} = [\vartheta(s) \cdot z_\infty]^2 \tag{4}$$

where f_{obj} is the objective function, $\vartheta(s)$ is the important feature, z_∞ is the ensemble of the field variation part, and $[\vartheta(s) \cdot z_\infty]$ means inner product.

In this work, the discrete version of the POD, which is SVD [29], is used to identify the important features since the experimental data are usually collected at discrete values.

1. Singular Value Decomposition

Assume that the spatiotemporal data matrix $\boldsymbol{X} \in \mathbb{R}^{m\times n} = [x(s_i,t_j)]$, $\forall\ i = 1, 2, \cdots, m;\ j = 1, 2, \cdots, n;$ is available, where $x(s_i,t_j)$ represents the value of X at the ith spatial location and the jth time instant, m indicates the number of spatial locations, and n indicates the number of time instants. This matrix can be scaled for the sake of further analysis as

$$\boldsymbol{Z} = \boldsymbol{X} - \boldsymbol{\mu}\boldsymbol{I}_{1\times n} \tag{5}$$

where $\mu(s_i) = \sum_{j=1}^{n} x(s_i,t_j)/n$, $i = 1, 2, \cdots, m$, $\boldsymbol{\mu} = [\mu(s_1), \mu(s_2), \cdots, \mu(s_m)]^T \in \mathbb{R}^{m\times 1}$ is the vector of mean values and $\boldsymbol{I}_{1\times n}$ is a vector of 1s.

Using the SVD method, the matrix $\boldsymbol{Z}$ can be decomposed into three matrices as [29]

$$\boldsymbol{Z} = \boldsymbol{V}\boldsymbol{H}\boldsymbol{U}^T \tag{6}$$

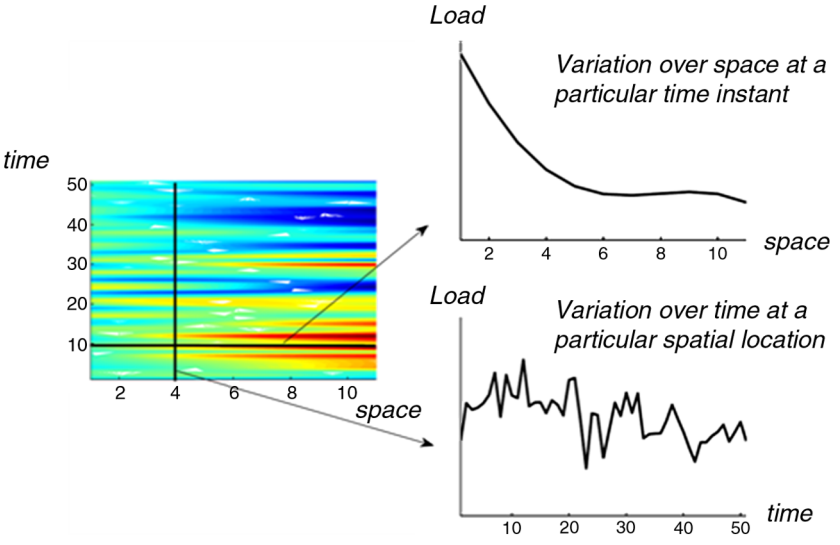

Fig. 3 Snapshot of a spatiotemporal random field.

where $\boldsymbol{V}$ is a matrix of order $m \times m$, $\boldsymbol{H}$ is a matrix of order $m \times n$, and $\boldsymbol{U}$ is a matrix of order $n \times n$. The matrix $\boldsymbol{H}$ contains singular values along the diagonal.

Let r_n be the number of important features, that is, the number of singular values that contribute 99% or more to the total sum. This is generally much smaller than the total number of singular values. The matrix $\boldsymbol{X}$ can now be rewritten as

$$x(:, t_i) = \mu(:) + \sum_{j=1}^{r_n} w_j(t_i)\vartheta_j \tag{7}$$

where $w_j(t_i) = A(i, j)$, $\boldsymbol{A} = \boldsymbol{VH}$, and ϑ_j is the jth row of $U(:, 1:r_n)^T$. It may be noted that the coefficients obtained through SVD decomposition are random variables in the absence of temporal variation and random processes in the presence of temporal variation and thus account for spatial variation, too.

2. SVD-Based Modeling of Spatiotemporal Variability

Using Eq. (7), the spatiotemporal data matrix $\boldsymbol{X}$ has now been decomposed into temporal and spatial parts, $w_j(t_i)$ and ϑ_j, respectively. The basis vectors that account for the correlation of the response over space are ϑ_j, and $w_j(t_i)$ represents the variation of the response over time. To consider the correlation among the snapshots over time, in this work, we propose to integrate a time-series model with SVD. More specifically, we use the time-series model to represent the variation over time and predict the future realizations using the time-series model.

Data-driven time-series models have been widely used in many areas, such as economics [30], finance [31], and weather forecasting [32], for the modeling of stochastic processes, especially for problems in which available realizations of the stochastic process are limited to one or just a few trajectories. The commonly used time-series models include the autoregressive (AR) model [33], moving average (MA) model [34], and ARMA model [34], which are suitable for stationary stochastic processes. When the stochastic process is nonstationary, the autoregressive integrated moving average (ARIMA) model is employed [34]. In this work, we focus on stationary temporal variations, and therefore the ARMA model is used. However, the developed method can be easily extended to problems with nonstationary time history using ARIMA. An ARMA (p, q) time-series model $Y_j(t)$ is given by

$$\begin{aligned} Y_j(t_i) = {} & \varphi_j^{(0)} + \varphi_j^{(1)} Y_j(t_{i-1}) + \varphi_j^{(2)} Y_j(t_{i-2}) + \cdots \\ & + \varphi_j^{(p)} Y_j(t_{i-p}) + \varepsilon_j(t_i) + \omega_j^{(1)} + \varepsilon_j(t_{i-1}) + \cdots \\ & + \omega_g^{(q)} \varepsilon_j(t_{i-q}) \end{aligned} \tag{8}$$

in which $\varepsilon_j(t_i), \varepsilon_j(t_{i-1}), \cdots, \varepsilon_j(t_{i-q})$ is a sequence of independent and identically distributed random variables with zero mean and finite standard deviation $\sigma_{j,t}$; $\varphi_j^{(0)}, \varphi_j^{(1)}, \cdots, \varphi_j^{(p)}$ are the coefficients of the AR term; $\omega_j^{(1)}, \cdots, \omega_j^{(q)}$ are the coefficients of MA term in the time-series model $Y_j(t)$; and p and q are the orders of the AR and MA terms, respectively.

Since each value of $w_j(t_i)$, $j = 1, 2, \cdots, r_n$, corresponds to a snapshot at specific time instant t_i of the random field [as indicated in Eq. (7)], the ARMA model is employed to model $w_j(t_i)$, $j = 1, 2, \cdots, r_n$. The number of ARMA models required is equal to the number of important features r_n. An ARMA model of order (p, q) for the time-series data $w_j(t)$, $j = 1, 2, \cdots, r_n$, can be represented as

$$w_j(t) = \varepsilon_{j,t} + \sum_{i=1}^{p} \varphi_j^{(i)} w_j(t-i) + \sum_{k=1}^{q} \omega_j^{(k)} \varepsilon_{j,t-k} \tag{9}$$

Note that the noise terms, $\varepsilon_j(t_i), \varepsilon_j(t_{i-1}), \cdots, \varepsilon_j(t_{i-q})$, are usually assumed to be independent and identically distributed (I.I.D.) and follow Gaussian distributions. They can also be modeled as non-Gaussian distributions. The non-Gaussian noise term, however, will make the modeling of ARMA models much more complicated [35]. In the following discussion, unless otherwise mentioned, they are assumed to follow Gaussian distributions for the sake of illustration. All the parameters of the ARMA model are unknown, and they need to be estimated based on available data. Many methods are available to estimate these parameters, such as the Yule–Walker method, Burg method, covariance method, and maximum likelihood estimation method [34,36]. Since the SVD method is used to obtain the important features and the ARMA model is used to represent the coefficients of the important features, we call the integrated model the SVD–ARMA model [37,38].

The SVD–ARMA model can effectively represent the spatiotemporal variability when we have enough observation data. However, the data available for $w_j(t_i)$, $j = 1, 2, \cdots, r_n$ (obtained from SVD) are usually sparse. As a result, estimates of the previously mentioned parameters of the ARMA models $(\varphi_j^{(1)}, \varphi_j^{(2)}, \ldots, \varphi_j^{(p)}, \omega_j^{(1)}, \omega_j^{(2)}, \ldots, \omega_j^{(q)}, \sigma_{j,t})$ are uncertain. This uncertainty about the actual value of the model parameter is termed epistemic uncertainty. In the following section, Bayesian calibration is used to quantify the epistemic uncertainty in the SVD–ARMA model and is discussed in detail.

3. Modeling of Epistemic Uncertainty

Bayesian calibration is used to update our belief about a quantity of interest when new evidence or observation is available. For a vector of calibration parameters $\boldsymbol{\theta}$, the posterior distribution of the calibration parameters is computed using Bayes's theorem as

$$f''(\boldsymbol{\theta}|\boldsymbol{D}) = L(\boldsymbol{\theta}) f'(\boldsymbol{\theta}) \Big/ \int L(\boldsymbol{\theta}) f'(\boldsymbol{\theta})\, \mathrm{d}\boldsymbol{\theta} \tag{10}$$

where $\boldsymbol{D}$ is the observation data, $f'(\boldsymbol{\theta})$ is the prior distribution, $f''(\boldsymbol{\theta}|\boldsymbol{D})$ is the posterior distribution, and $L(\boldsymbol{\theta})$ is the likelihood function. The likelihood function is a measure of how well the observation data support the current belief regarding the calibration parameters.

Directly solving the previous equation is difficult when the dimension of $\boldsymbol{\theta}$ is high. In that case, Markov chain Monte Carlo (MCMC) sampling [39] is widely used to estimate Eq. (10) based on the proportional relationship

$$f''(\boldsymbol{\theta}|\boldsymbol{D}) \propto L(\boldsymbol{\theta}) f'(\boldsymbol{\theta}) \tag{11}$$

where $\propto$ stands for "proportional to." For the sake of illustration, we denote all the parameters in the ARMA model given in Eq. (8) as $\boldsymbol{\theta}_j = [\sigma_\varepsilon, \varphi_j^{(1)}, \varphi_j^{(2)}, \cdots, \varphi_j^{(p)}, \omega_j^{(1)}, \omega_j^{(2)}, \cdots, \omega_j^{(q)}]$, $\forall\ j = 1, 2, \cdots, r_n$.

A critical step for the application of Bayesian calibration is the computation of the likelihood function $L(\boldsymbol{\theta}_j)$. For given values of $\boldsymbol{\theta}_j$ and I.I.D noise terms (with Gaussian distribution), $L(\boldsymbol{\theta}_j)$ is given by [40]

$$L(\boldsymbol{\theta}_j) = (2\pi\sigma_t^2)^{-(n-p)/2} \exp\left[-\sum_{t=p+1}^{n} e_t^2/(2\sigma_t^2) \right] \tag{12}$$

where

$$e_t = w_j(t) - \sum_{i=1}^{p} \varphi_j^{(i)} w_j(t-i) - \sum_{k=1}^{q} \omega_j^{(k)} \varepsilon_{t-k} \tag{13}$$

With the likelihood function, the posterior distribution of the parameters of each ARMA model is obtained using MCMC based on Eq. (11). The spatiotemporal variability with epistemic uncertainty is then represented as $x(s, t, \boldsymbol{\theta}_1, \boldsymbol{\theta}_2, \cdots, \boldsymbol{\theta}_{r_n})$. Note that $\boldsymbol{\theta}_1, \boldsymbol{\theta}_2, \cdots, \boldsymbol{\theta}_{r_n}$ are the coefficients of $w_j(t_i)$, $j = 1, 2, \cdots, r_n$. In the following sections, for the sake of illustration, we use $\boldsymbol{\Theta} = [\boldsymbol{\theta}_1, \boldsymbol{\theta}_2, \cdots, \boldsymbol{\theta}_{r_n}]$ to represent all the coefficients, and we have $x(s, t, \boldsymbol{\Theta})$.

B. Snap-Through Buckling Reliability Analysis

In this section, we discuss the snap-through buckling reliability analysis by considering the spatiotemporal variability and epistemic uncertainty. Defining the critical buckling load for structures under loads with spatiotemporal variability is difficult. The reason is that if the loads are randomly distributed there are numerous values of loads the structure is experiencing at the same time, but the critical buckling load is a single value. A common strategy in deterministic buckling analysis is to consider proportional loading. i.e., assume a load distribution over space and gradually increase the load proportionally over the structure (keeping the same load profile) to identify the load proportionality factor (lpf) at which buckling occurs. However, when the load has spatial randomness, many realizations of the load profile are possible, and the load proportionality factor needs to be identified for each profile. Additional variability in material properties and boundary conditions requires additional random realizations of these quantities and affects lpf.

For the curved beam example discussed in Sec. IV, the lpf obtained for various realizations of the random quantities are shown in Fig. 4. Two-dimensional contour plots for only a few variables are shown in Fig. 4 as illustration, where ξ_1 and ξ_2 represent spatial randomness of thickness h, and w_1 and w_2 are parameters of the load history (described in detail later in Sec. IV). It can be seen that the response is highly irregular and nonlinear, which makes it difficult to use commonly used numerical surrogate models such as the Gaussian process or PCE.

Since we cannot use numerical surrogate models to build a response surface for the critical load, we cannot directly use the limit-state function given in Eq. (1) for the buckling reliability analysis with spatiotemporal variability and epistemic uncertainty. Thus, instead of a general-purpose numerical surrogate model, we pursue the construction of a classification surrogate model. We first define a failure indicator function as

$$I_b[\boldsymbol{X}, \boldsymbol{X}_F, \boldsymbol{X}(s,t,\boldsymbol{\Theta})] = \begin{cases} 1, & \text{buckling occurs} \\ 0, & \text{otherwise} \end{cases} \tag{14}$$

where $\boldsymbol{X}$ is the vector of random quantities in the buckling analysis model, $\boldsymbol{X}_F$ is the random field model with only spatial variability such as the material properties, and $\boldsymbol{X}(s,t,\boldsymbol{\Theta})$ is the spatiotemporal variability conditioned on the ARMA parameters $\boldsymbol{\Theta}$, which are obtained from experimental or operational data. The failure indicator function for the snap-through buckling problem can be obtained either by comparing lpf with a threshold value or using clustering. Although comparing with a threshold is a commonly used technique, more often than not, it may not be possible to define a threshold value [17,41].

For the current snap-through buckling problem, either of the previous two techniques can be used. For comparing with a threshold, the initial load profile is divided by a number, say lpf_0; the analysis starts from this load profile. It is clear that if lpf exceeds lpf_0 then buckling occurs, and thus lpf_0 is the threshold value. An alternative method is to obtain the midpoint displacement of the beam with the initial load profile. A large displacement indicates that the beam has failed and vice versa. This results in a discontinuity in the displacement response surface. K-means clustering similar to that used by Basudhar and Missoum [41] can be used to identify the two classes, one corresponding to the case in which the beam buckles and the other to the case in which the beam is safe. The K-means clustering technique identifies the various classes through discontinuities in the response surface. In the current work, we use the threshold technique to identify if the beam has buckled or not due to its simplicity and accuracy.

Based on the definition of the failure indicator function, the buckling failure probability is defined as

$$p_f(\boldsymbol{\Theta}) = Pr\{I_b[\boldsymbol{X}, \boldsymbol{X}_F, \boldsymbol{X}(s,t,\boldsymbol{\Theta})] = 1, \exists\ t \in [t_0, t_e]\} \tag{15}$$

in which $p_f(\boldsymbol{\Theta})$ is the failure probability conditioned on the realization of the epistemic variables $\boldsymbol{\Theta}$, $\exists$ stands for "there exists," and t_0 and t_e are the initial and last time instants of the time period of interest. Here, the probability of failure for a time interval $[t_0, t_e]$ is defined as the probability that the system snaps through in that time interval. No vibratory loads are considered in the current study. Instead, we consider the quasi-static load to be varying randomly over the given time interval. The resulting failure probability thus accounts for the worst possible quasi-static loading condition and does not include dynamic amplification in vibratory loads; however, the overall reliability analysis procedure is the same if dynamic amplification is included.

The unconditional buckling failure probability is given by

$$p_f = \int p_f(\boldsymbol{\Theta}) f''(\boldsymbol{\Theta})\, \mathrm{d}\boldsymbol{\Theta} \tag{16}$$

in which $f''(\boldsymbol{\Theta})$ is the posterior distribution of $\boldsymbol{\Theta}$ obtained using Bayes' theorem as indicated in Eq. (11).

The failure probability given in Eq. (15) is the time-dependent failure probability [42,43], which gives us the probability of failure over the time interval of interest $[t_0, t_e]$. Here, the time-dependent failure probability is used due to the temporal variability. Directly solving Eqs. (15) and (16) is computationally very expensive because the indicator function given in Eq. (14) usually needs to be evaluated using simulation models. For a given realization of $\boldsymbol{X} = \boldsymbol{x}, \boldsymbol{X}_F = \boldsymbol{x}_F$, and $\boldsymbol{X}(s,t,\boldsymbol{\Theta}) = \boldsymbol{x}(s,t,\boldsymbol{\Theta})$, a buckling simulation is performed to see whether snap-through buckling occurs or not. To save the computational cost of buckling reliability analysis, we construct a SVM-based classifier; thus, a SVM is a classification surrogate model. In the following sections, we first briefly review the SVM method. We then discuss buckling reliability analysis using a SVM.

1. *Support Vector Machine*

In building a SVM classifier, we construct the best hyperplane that separates two classes of data [44]; this is an optimization problem as illustrated in Fig. 5. Consider two input variables, p_1 and p_2. The output, which is a function of these two variables, can be classified into either the $+1$ class or the -1 class. Let al. the data belonging to class $+1$ lie to the left of line A. Similarly, all data belonging to class -1 lie to the right of the line C. Line B is equidistant from both A and C. Now, the objective is to obtain the best separating hyperplane, B, such that the distance between the lines A and C is maximized [44].

Let $\boldsymbol{d}$ be any vector in the (p_1, p_2) plane. The equation of the hyperplane B can be given as

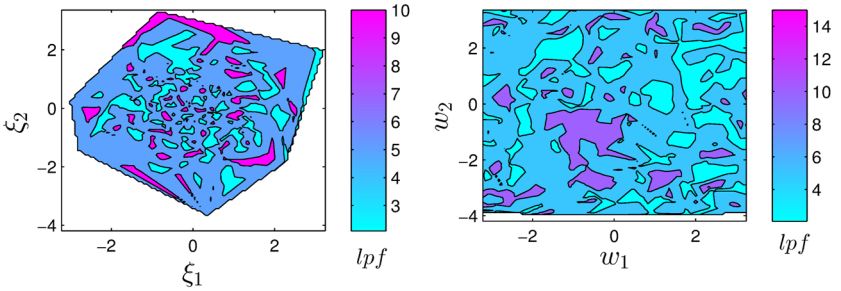

Fig. 4 Two-dimensional plots of lpf with respect to realizations of a few random quantities (defined in Sec. IV).

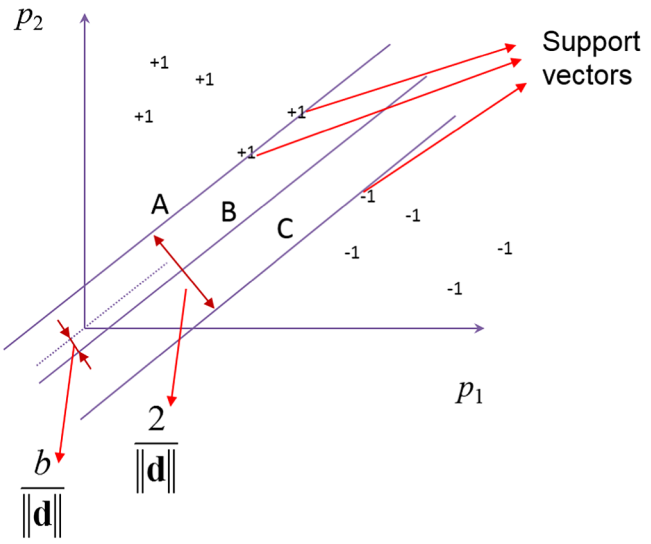

Fig. 5 Support vector machine.

$$\boldsymbol{p} \cdot \boldsymbol{d} - b = 0 \tag{17}$$

where $\cdot$ stands for inner product, $\boldsymbol{d}$ is any vector, and b is any scalar.

Similarly, the equations of the hyperplanes A and C can be respectively given as [44]

$$\boldsymbol{p} \cdot \boldsymbol{d} - b = +1 \tag{18}$$

$$\boldsymbol{p} \cdot \boldsymbol{d} - b = -1 \tag{19}$$

Therefore, the distance between A and C can be given as $2/\|\boldsymbol{d}\|$. To maximize this distance, we have to minimize $\|\boldsymbol{d}\|$. It may also be noted that, by virtue of Eqs. (18) and (19), for all data that belong to class $+1$,

$$(\boldsymbol{d} \cdot \boldsymbol{p}_i) - b \geq 1 \tag{20}$$

and for all data that belong to class -1,

$$(\boldsymbol{d} \cdot \boldsymbol{p}_i) - b \leq -1 \tag{21}$$

Equations (20) and (21) can be combined together as [44]

$$y_i[(\boldsymbol{d} \cdot \boldsymbol{p}_i) - b] \geq 1 \tag{22}$$

where y_i is the data class at point $\boldsymbol{p}_i$. The previous discussion can be cast into a mathematical optimization problem as [44]

$$\min_{d,b} \boldsymbol{d} \cdot \boldsymbol{d}/2 \quad \text{s.t. } y_i[(\boldsymbol{d} \cdot \boldsymbol{p}_i) - b] \geq 1 \tag{23}$$

where "s.t." stands for "such that."

We can also rewrite Eq. (14) using the definition of y_i as

$$I_b[\boldsymbol{X}, \boldsymbol{X}_F, \boldsymbol{X}(s,t,\boldsymbol{\Theta})] = \frac{y_i + 1}{2} \tag{24}$$

It may be noted that the previous discussion is only for data that can be separated, meaning that the data can be clearly identified as belonging to either class -1 or class $+1$. However, in practical applications, the data may be nonseparable as shown in Fig. 6; i.e., data belonging to one class are occasionally found within the general domain of the other class.

In such cases, a soft margin (using slack variables) is used within the SVM approach. This indicates that most, but not all, data points are separated. For nonseparable data, the optimization problem can be cast as [44]

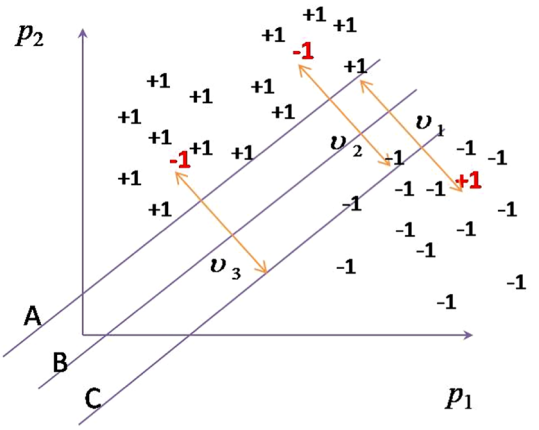

Fig. 6 Nonseparable data.

$$\min_{d,b,\upsilon_i} \frac{1}{2}\boldsymbol{d} \cdot \boldsymbol{d} + C_{mc}\sum_i \upsilon_i \quad \text{s.t. } y_i[(\boldsymbol{d} \cdot \boldsymbol{p}_i) - b] \geq 1 - \upsilon_i, \quad \upsilon_i \geq 0 \tag{25}$$

where υ_i are the slack variables and give the distance from the misclassified point to one of the lines A or C and C_{mc} is the weight acting on the slack variables and represents how much misclassification is permitted. Once the best separating hyperplane has been obtained, any point can be classified into either of the classes by estimating its classification score. For any point $\boldsymbol{p}$, the classification score cs_i can be given as $\boldsymbol{d} \cdot \boldsymbol{p} - b$, and its class is given by $\text{sign}(\boldsymbol{d} \cdot \boldsymbol{p} - b)$.

More often than not, the data available may not be amenable to linear classification. In such cases, kernel functions may be used to transform low-dimensional nonlinear data into a higher-dimensional linearly classifiable data [41,45]. Constructing a nonlinear classification boundary is not difficult; however, nonseparable data, i.e., the presence of small islands of data belonging to one class within a larger domain of the other class is a challenge for numerical response surface models that attempt to model a physical quantitative output. Such models will require a highly nonlinear function and a large number of training points to capture the islands accurately. This is where the slack variable approach of the SVM classification surrogate model gives it a distinct advantage over numerical surrogate models of physical outputs, and is found to be useful in buckling reliability analysis, thus addressing the situation in Figs. 4 and 7.

One of the important challenges in successfully using an SVM classifier is to choose the right values of the parameters; for example, the weight acting on the slack variables C_{mc} can be obtained through optimization to minimize the misclassification percentage. Jiang et al. [46] have used three different metrics, namely, accuracy, balanced accuracy, and the area under the receiver operating characteristic curve, to optimally obtain the various SVM parameters. In the current work, we use the default values of the parameters in the MATLAB® in-built SVM classification function fitcsvm and also the parameters of fitPosterior, which estimates the classification uncertainty. However, optimizing the parameters may result in a more accurate SVM classifier and can be considered in future extensions of this methodology.

2. *Buckling Reliability Analysis Using SVM*

We now discuss how to use SVM to perform snap-through buckling reliability analysis with spatiotemporal variability and epistemic uncertainty. In the buckling reliability analysis, as indicated in Eq. (15), we may have random variables $\boldsymbol{X}$, a random field $\boldsymbol{X}_F$, and spatiotemporal variability $\boldsymbol{X}(s,t)$. The spatiotemporal variability is modeled using the SVD–ARMA model as discussed in Sec. III.A. The random field $\boldsymbol{X}_F$ with only spatial variability is usually modeled using the Karhunen–Loeve (KL) expansion method as [47]

$$X_F(s) = \mu(s) + \sum_{i=1}^{n_F} \sqrt{\lambda_i}\,\xi_i^F f_i(s) \tag{26}$$

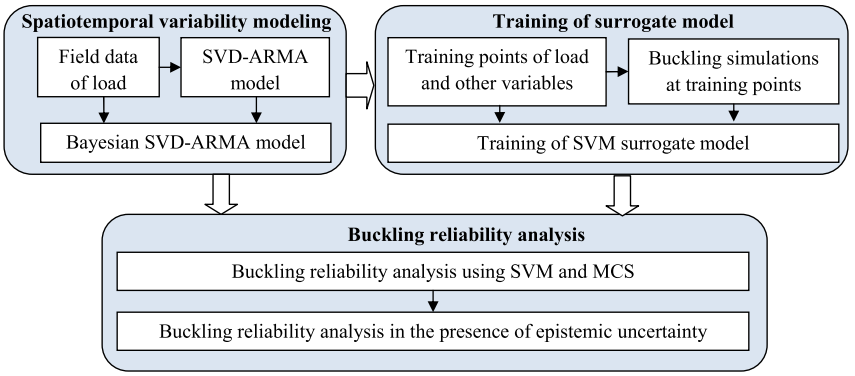

Fig. 7 Bayesian calibration of ARMA model parameters for the three load coefficients.

where λ_i and $f_i(s)$ are the eigenvalues and eigenfunctions of the covariance function of the random field and ξ_i^F, $i = 1, 2, \cdots, n_F$, are independent random variables.

After replacing $\boldsymbol{X}_F$ with ξ_i^F, $i = 1, 2, \cdots, n_F$, the snap-through buckling reliability given in Eq. (15) is written as

$$p_f(\boldsymbol{\Theta}) = Pr\{I_b[\boldsymbol{X}, \boldsymbol{\xi}^F, \boldsymbol{X}(s, t, \boldsymbol{\Theta})] = 1, \exists\ t \in [t_0, t_e]\} \tag{27}$$

where $\boldsymbol{\xi}^F = [\xi_1^F, \xi_2^F, \cdots, \xi_{n_F}^F]$.

A straightforward way of using the SVM to estimate the failure probability given in Eq. (27) is to train a SVM model for the failure indicator function defined in Eq. (14) as a function of $\boldsymbol{X}$, $\boldsymbol{\xi}^F$, and $\boldsymbol{\Theta}$. The dimensionality of $\boldsymbol{\Theta}$, however, may be high. To reduce the dimensionality, we train the SVM model as a function of $\boldsymbol{X}$, $\boldsymbol{\xi}^F$, and $\boldsymbol{w} = [w_1(t), w_2(t), \cdots, w_{r_n}(t)]$ [the coefficients of the SVD model as indicated in Eq. (7)]. The general procedure of snap-through buckling reliability analysis is explained as follows:

1) Model the spatiotemporal variability of the quantity of interest using the SVD–ARMA model and quantify the epistemic uncertainty in the SVD–ARMA model using Bayesian calibration.

2) Generate training points for $\boldsymbol{X}$, $\boldsymbol{\xi}^F$, and $\boldsymbol{w} = [w_1(t), w_2(t), \cdots, w_{r_n}(t)]$ using Latin hypercube sampling.

3) Convert $\boldsymbol{\xi}^F$ into random field quantity $\boldsymbol{X}_F$ using Eq. (26) and $\boldsymbol{w} = [w_1(t), w_2(t), \cdots, w_{r_n}(t)]$ into $\boldsymbol{X}(s, t)$ using Eq. (7).

4) Perform snap-through buckling analysis at the training points using finite-element analysis, and thus obtain the failure indicator responses $I_b[\boldsymbol{X}, \boldsymbol{X}_F, \boldsymbol{X}(s, t)]$.

5) Train a SVM surrogate model for the failure indicator, and represent the surrogate model as $y_{\text{buckling}} = \hat{I}_b(\boldsymbol{X}, \boldsymbol{\xi}^F, \boldsymbol{w})$.

6) Generate samples of $\boldsymbol{w}$ using the ARMA models developed in Step 1 and samples of $\boldsymbol{X}$ and $\boldsymbol{\xi}^F$. Note that if the unconditional failure probability as given in Eq. (16) is desired the unconditional samples of $\boldsymbol{w}$ need to be generated by considering the variability in the posterior distribution of $\boldsymbol{\Theta}$.

7) Obtain the indicator responses by substituting the samples of $\boldsymbol{w}$, $\boldsymbol{X}$, and $\boldsymbol{\xi}^F$ into $y_{\text{buckling}} = \hat{I}_b(\boldsymbol{X}, \boldsymbol{\xi}^F, \boldsymbol{w})$ into the SVM model. Suppose the indicator responses at the samples are given by

$$\boldsymbol{y}_{\text{buckling}} = \begin{bmatrix} y_{\text{buckling}}(1,1) & y_{\text{buckling}}(1,2) & \cdots & y_{\text{buckling}}(1,n) \\ y_{\text{buckling}}(2,1) & y_{\text{buckling}}(2,2) & \cdots & y_{\text{buckling}}(2,n) \\ \vdots & \vdots & \ddots & \vdots \\ y_{\text{buckling}}(N,1) & y_{\text{buckling}}(N,2) & \cdots & y_{\text{buckling}}(N,n) \end{bmatrix} \tag{28}$$

where N is the number of samples at each time instant, n is the number of time instants into which the time interval of interest $[t_0, t_e]$ is discretized, and $y_{\text{buckling}}(i, j)$ is the indicator response of the ith sample at the jth time instant.

The failure probability is then computed as

$$p_f = \sum_{i=1}^{N} \max_j \{y_{\text{buckling}}(i, j)\}/N \tag{29}$$

3. *Reliability Analysis Under Epistemic Uncertainty*

Two sources of epistemic uncertainty involved in buckling reliability analysis are considered here, namely, data uncertainty and surrogate model uncertainty. An important additional source of epistemic uncertainty is the physics model uncertainty; this is not considered in this paper. The two epistemic uncertainty sources considered here are related to limited data; the first one relates to limited physical data available to characterize spatiotemporal variability, and the second one relates to limited training data for the SVM surrogate model due to computational expense. In this section, we discuss how to incorporate these two sources of epistemic uncertainty in reliability analysis.

a. Incorporation of Data Uncertainty. The epistemic uncertainty in the SVD–ARMA model (coefficients of ARMA models) due to limited data is represented through probability distributions using the Bayes's theorem as discussed in Sec. III.A. A straightforward way of incorporating the data uncertainty into reliability analysis is to employ a double-loop implementation procedure. The basic procedures of the double-loop framework are summarized as follows:

1) Generate the values of ARMA parameters from their posterior distributions.

2) Perform buckling reliability analysis (Sec. III.B) conditioned on each sample of the ARMA parameters. The conditional failure probability is obtained as in Eq. (15). Based on this, the unconditional buckling failure probability is obtained using Eq. (16).

The previously mentioned double-loop procedure, however, is computationally expensive since the time-dependent buckling reliability analysis needs to be performed repeatedly for each realization of the ARMA parameters. To improve the efficiency, an auxiliary variable approach that converts the double-loop procedure into a single-loop procedure is employed in this paper.

In the auxiliary variable approach, an auxiliary variable is defined such that the variability in the ARMA model can be explicitly represented as a deterministic function of cumulative distribution function (CDF) values (aleatory randomness) and epistemic parameters so that the double-loop procedure can be replaced by the single-loop approach. At each time instant, the ARMA model is a random variable. For a given ARMA model $w_i(t_j)$ at time instant t_j, the probability density function of $w_i(t_j)$ is $f_w(w|\boldsymbol{\Theta})$, and the CDF value u is given by [48]

$$u = \int_{-\infty}^{w} f_w(x|\boldsymbol{\Theta})\, \mathrm{d}x \tag{30}$$

where x is a dummy variable for integration. Repeating the same procedure [Eq. (30)] by considering the variability of $w_i(t_j)$, we will get corresponding CDF values. The obtained CDF values define

another random variable U_i, which follows a uniform distribution on [0, 1]. For a given value of $U_i = u$ and given values of $\boldsymbol{\Theta}$, there is a one-to-one mapping to the realization of $w_i(t_j)$. More details about the auxiliary variable approach are given by Sankararaman and Mahadevan [48], and adaptation of this approach to reliability analysis is discussed by Nannapaneni and Mahadevan [49].

Using the auxiliary variable approach, a realization of $w_i(t_j)$ for a given $U_i = u$ and $\boldsymbol{\Theta}$ can be computed by

$$w = F_w^{-1}(U_i = u|\boldsymbol{\Theta}) \tag{31}$$

where $F_w^{-1}(\cdot)$ is the inverse CDF of $w_i(t_j)$. Note that the previous equation is a deterministic relationship.

Defining an auxiliary variable for each time instant, the double-loop procedure then becomes a single-loop procedure as follows:

1) Generate the values of ARMA parameters from their posterior distributions and random samples for the auxiliary variables. Convert the samples of ARMA parameters and auxiliary variables into realizations of spatiotemporal variability.

2) Obtain the buckling indicator responses at the realizations of spatiotemporal variability, and thus directly compute the unconditional buckling failure probability.

Further, since the computer simulations are often computationally expensive, the SVM model may not be well trained due to limited computational resources. In that situation, the classification uncertainty will affect the time-dependent reliability analysis results. Next, we will discuss how to incorporate the effect of classification uncertainty on the reliability estimate.

b. Incorporation of Classification Uncertainty. The SVM classifier that has been discussed previously is based on the assumption that there is no uncertainty in the classification of the data to either of the classes. However, since the SVM is constructed using a limited number of training data, any new classification is inherently uncertain. Thus, for any new point that needs to be classified, we can associate a probability of it belonging to class $+1$ or class -1. The classification uncertainty P_C can be obtained from the classification score using the following two different transformation functions [44]. For separable data, a discrete transformation function is available,

$$P_C(\mathrm{cs}_i) = \begin{cases} 0; & \mathrm{cs}_i < \max\limits_{y_k=-1} \mathrm{cs}_k, \\ \pi_C; & \max\limits_{y_k=-1} \mathrm{cs}_k \le \mathrm{cs}_i \le \min\limits_{y_k=1} \mathrm{cs}_k, \\ \pi_C; & \mathrm{cs}_i > \min\limits_{y_k=1} \mathrm{cs}_k \end{cases} \tag{32}$$

where P_C is the probability of $\boldsymbol{p}_i$ falling into class $+1$ and π_C indicates the prior probability of class $+1$. The prior probability is obtained from the training data. For nonseparable data, a sigmoid function is available for estimating classification uncertainty,

$$P_C(\mathrm{cs}_i) = \frac{1}{1 + \exp(S\mathrm{cs}_i + I)} \tag{33}$$

in which S and I are the slope and the intercept; both can be obtained from the training data using logistic regression [44].

After introducing the classification uncertainty into buckling reliability analysis, each indicator response given in Eq. (28) is a binary random variable with probability given in Eq. (32) or Eq. (33). For any specific indicator response $y_{\text{buckling}}(i, j), \forall\ i = 1, 2, \cdots, N$; $j = 1, 2, \cdots, m$, we have

$$\begin{cases} Pr\{y_{\text{buckling}}(i, j) = 0\} = 1 - P_C \\ Pr\{y_{\text{buckling}}(i, j) = 1\} = P_C \end{cases} \tag{34}$$

Equation (34) implies that the buckling failure probability given in Eq. (29) is a random variable due to the uncertainty in $y_{\text{buckling}}(i, j)$. A bootstrapping approach can be employed to quantify the uncertainty in p_f due to the classification uncertainty. The basic idea is to generate samples of $y_{\text{buckling}}(i, j)$ based on the classification probability given in Eq. (34). Based on the samples of $y_{\text{buckling}}(i, j)$, samples of p_f are obtained. Suppose that N_c samples are generated for each $y_{\text{buckling}}(i, j)$ based on the classification uncertainty; we then have

$$\boldsymbol{y}_{\text{buckling}}^{(i)} = \begin{bmatrix} y_{\text{buckling}}^{(i)}(1,1) & y_{\text{buckling}}^{(i)}(1,2) & \cdots & y_{\text{buckling}}^{(i)}(1,m) \\ y_{\text{buckling}}^{(i)}(2,1) & y_{\text{buckling}}^{(i)}(2,2) & \cdots & y_{\text{buckling}}^{(i)}(2,m) \\ \vdots & \vdots & \ddots & \vdots \\ y_{\text{buckling}}^{(i)}(N,1) & y_{\text{buckling}}^{(i)}(N,2) & \cdots & y_{\text{buckling}}^{(i)}(N,m) \end{bmatrix}, \quad \forall\ i = 1, 2, \cdots, N_c \tag{35}$$

where $y_{\text{buckling}}^{(i)}(j, k)$ is the ith sample of $y_{\text{buckling}}(j, k)$ generated based on Eq. (34).

Based on the samples of failure indicators, we have the samples of p_f as follows:

$$p_f^{(k)} = \sum_{i=1}^{N} \max_j \{y_{\text{buckling}}^{(k)}(i, j)\}/N, \quad \forall\ k = 1, 2, \cdots, N_c \tag{36}$$

The uncertainty in p_f due to the classification uncertainty is then quantified based on the random samples.

Until now, we have discussed the techniques required for the snap-through buckling reliability analysis under spatiotemporal variability and epistemic uncertainty. As shown in Fig. 8, the proposed method in general consists of three main parts. In the first part, the spatiotemporal variability is represented using an SVD–ARMA model, and the epistemic uncertainty in the spatiotemporal variability modeling is quantified in using the Bayesian calibration. In the second part, an SVM classifier surrogate model is constructed for the snap-through buckling failure event instead of the common practice of building a numerical surrogate model for the critical buckling load. In the third part, the SVD–ARMA model is integrated with the SVM model to perform time-dependent buckling reliability analysis, and the effects of surrogate model uncertainty on the reliability analysis results are quantified. These steps provide an effective strategy for snap-through buckling reliability analysis under both aleatory and epistemic uncertainty, in the presence of spatiotemporal variability in loads and structural properties. A numerical example is given in the subsequent section to demonstrate the proposed method.

IV. Numerical Example

A. Problem Description

A curved beam as shown in Fig. 2 with an uncertain boundary condition is used to demonstrate the proposed method. The force-deflection curve for this structure looks very similar to that shown in Fig. 1b. The Young modulus E is modeled as an aleatory lognormal random variable, and the thickness h is modeled as a random field with spatial variability. The modeling of thickness as a random field captures the issue of geometric imperfection, a factor often studied in the context of buckling. The load P varies over both space and time and is modeled based on assumed experimental data. The flexibility coefficient of the spring (at End 2 of the beam) K is assumed to be an aleatory random variable following a lognormal distribution. Table 1 describes the variables in this example.

The autocorrelation function of the thickness h random field is assumed to be given by

$$\rho_h(s, s') = \exp[-(s - s')^2/2l_h^2] \tag{37}$$

where $l_h = 2.5$ in. Based on the correlation function, the Young modulus is represented using the K–L expansion. Since just two eigenvalues add up to about 95% of the total sum of all the eigenvalues, only two terms are used in the K–L expansion. The reliability

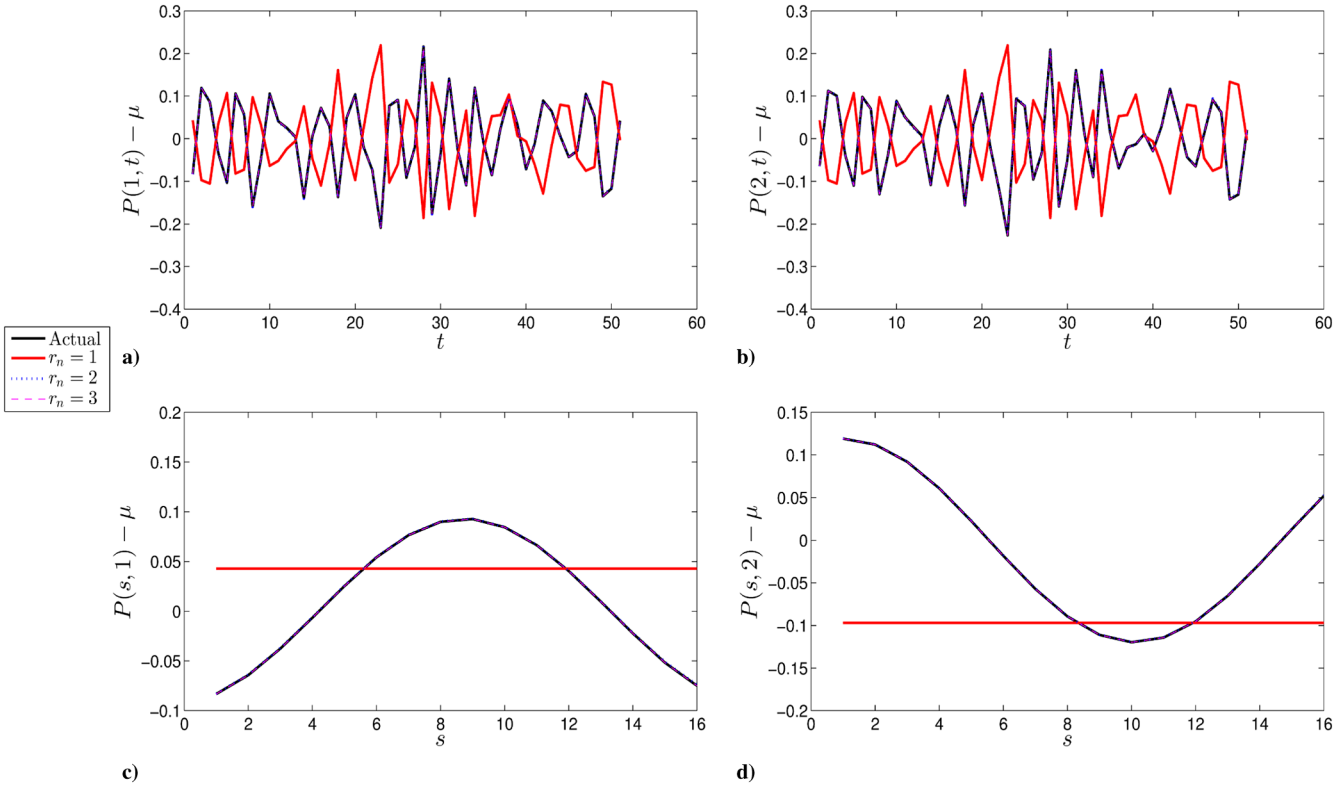

Fig. 8 Flowchart of the proposed buckling reliability analysis method.

of the curved beam with respect to snap-through buckling over [0, 50] min is estimated. Following the procedure of the proposed method, we first model the spatiotemporal variability of the load based on experiment data.

Note that epistemic uncertainty in K and E can also be included in the reliability analysis. K and E can be an unknown deterministic constant, an aleatory variable with unknown distribution type and parameters, or a random field with unknown correlation length and variance, all of which can be characterized using Bayesian calibration.

B. Representation of the Spatiotemporal Variability

It is assumed that the spatiotemporal load data is available at 16 spatial locations on the beam and at 51 time instants. The data are first processed using SVD as discussed in Sec. III.A. Because of the space limitation, we do not give the detailed data here. Figure 9 shows the reconstruction of the load data using SVD. Figures 9a and 9b give the reconstructed load over time, and Figs. 9c and 9d depict the reconstructed loads over space. $P(1,t)$ and $P(2,t)$ represent the spatiotemporal load histories corresponding to two different spatial locations, and $P(s,1)$ and $P(s,2)$ represent the variation over space for two different time instants. It is found that the spatiotemporal load data can be almost perfectly reconstructed with the first three important features. In the SVD model, we therefore use three important features to model the load with spatiotemporal variability.

Since the first three important features are used in the SVD expansion, we need to model the three time-dependent coefficients, $w_1(t_i)$, $w_2(t_i)$, and $w_3(t_i)$, using ARMA models. We use ARMA models of order (1,1). However, they can be chosen using Bayesian calibration similar to how the other ARMA model parameters are chosen. A detailed description for calibrating the ARMA model parameters can be found in the work by Uturbey [40]. Let the parameters for these three models be represented as $\{\phi_1, \theta_1, \sigma_{1,t}\}$, $\{\phi_2, \theta_2, \sigma_{2,t}\}$, and $\{\phi_3, \theta_3, \sigma_{3,t}\}$. Using Bayesian calibration, the posteriors for these parameters are obtained by assuming uniform prior distributions. Figure 7 shows the prior and posterior distributions of the coefficients of the three ARMA models.

These parameters will be used to simulate the load history realizations during the time-dependent buckling reliability analysis.

Table 1 Variables in the curved beam example

Variable	Distribution	Mean	Standard deviation	Correlation
K	Lognormal	0.0098	0.0058	— —
h	Normal	0.0684 in.	0.00684 in.	Eq. (37)
E	Lognormal	$1e7$ lb/in.^{2}	$1e6$ lb/in.^{2}	— —
P	Modeled based on experimental data			

C. Time-Dependent Snap-Through Buckling Reliability Analysis

It may be noted that, even for a simple structure like the curved beam discussed in Sec. IV.A, the computational effort using Monte Carlo simulation (MCS) is already very large, since each run takes about 2 min on a desktop computer and MCS requires about 100,000 samples to converge. Therefore, following the procedure given in Sec. III.B, the SVM model is trained for the buckling failure indicator. Five hundred training points are generated for boundary condition K, Young's modulus E, the variables ξ_1 and ξ_2 in the K–L expansion of the thickness random field, and the coefficients of the ARMA load model. At each of the training points, snap-through buckling analysis is performed for the curved beam. Pass/fail data, as a function of the individual variables, are given in Fig. 10. It can be seen that the data are nonseparable; i.e., the data jump frequently between 0 and 1. The inseparability in each plot is of course due to the effect of the other variables; in seven-dimensional space, the points will be apart from each other, yet the situation shown in Fig. 4 is also present, requiring a highly nonlinear function to represent the data with load proportionality factor lpf as the output. In fact, a Kriging surrogate model was tried with the same training data, and the bias and variance in Kriging model prediction were found to be too large. On the other hand, the SVM approach does not attempt to model every island in the data; instead, slack variables are introduced to account for misclassification, resulting in satisfactory accuracy, efficiency, and uncertainty quantification.

Based on the trained SVM model, the time-dependent buckling failure probability is analyzed. Figure 11 gives the unconditional time-dependent buckling failure probability over the time interval of

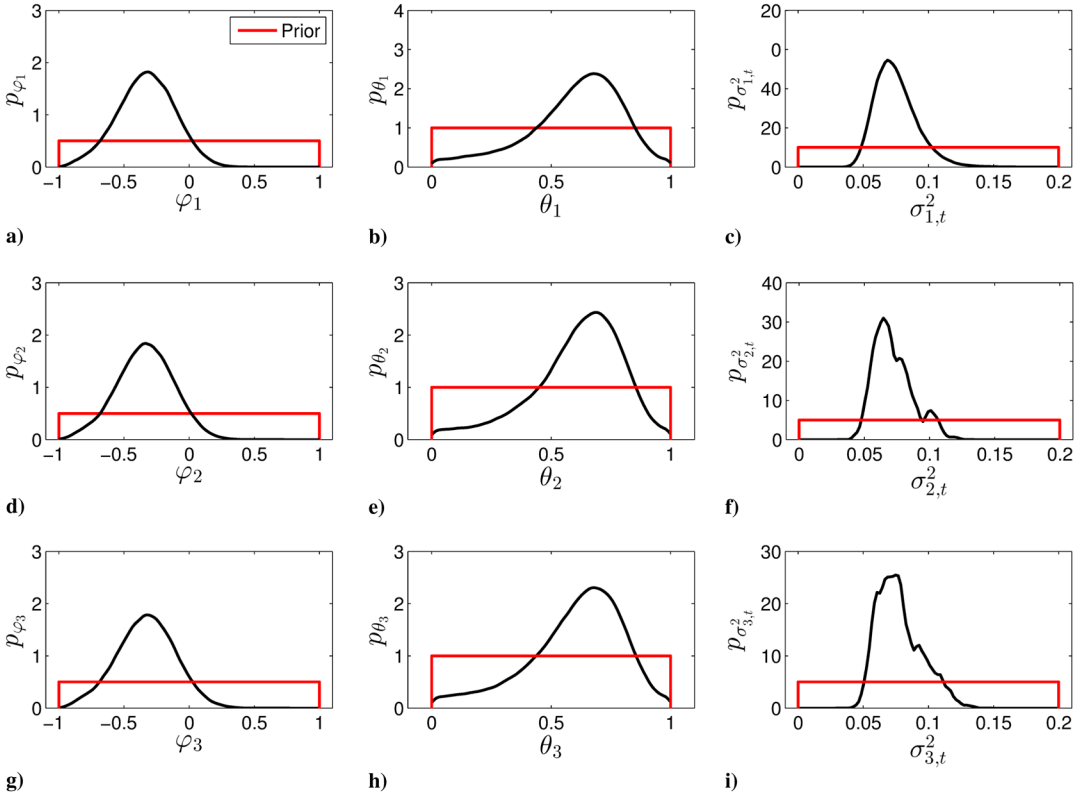

Fig. 9 Reconstruction of the spatiotemporal data using SVD.

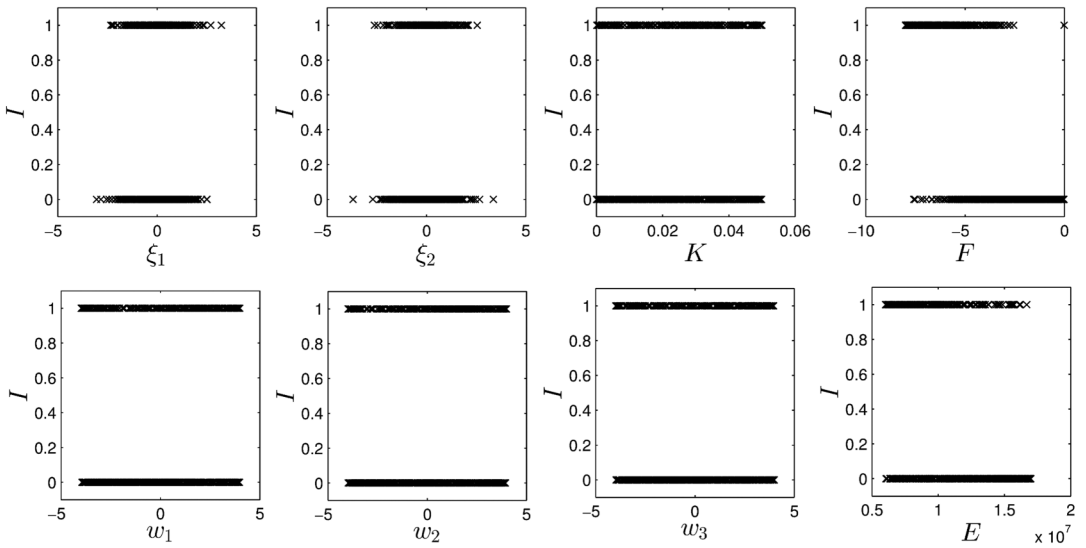

Fig. 10 Pass/fail data as a function of the random variables (units of E: lb/in.^{2}. Other quantities are dimensionless).

interest by assuming that there is no classification uncertainty in the surrogate model. It can be seen that the buckling failure probability increases with time due to the temporal variability of the load. It implies that the proposed method can effectively perform buckling reliability analysis for problems with spatiotemporal variability and epistemic uncertainty.

D. Buckling Failure Probability with Classification Uncertainty

Next, we quantify the uncertainty in the buckling failure probability estimate due to classification uncertainty caused by limited training data, by using the method presented in Sec. III.B. Figure 12 shows the buckling failure probability over the time interval of interest considering the classification uncertainty. It is to be noted that the failure probability obtained in the absence of classification uncertainty is lesser than the mean failure probability obtained in the presence of classification uncertainty. This could be attributed to the high misclassification percentage of about 3%. The misclassification percentage can be reduced by increasing the accuracy of the SVM model (either by increasing the number of training points or by optimizing the SVM parameters). It shows that the proposed method can not only provide a deterministic estimate of the buckling failure probability over time but also give the uncertainty bounds of the estimate due to the classifier uncertainty.

It is to be noted that the computational effort required for the proposed strategy is much less than that required for traditional MCS, which takes thousands of runs to converge. The number of training points required for the SVM classifier is 500. Quantification of epistemic uncertainty in the representation of spatiotemporal variability requires about 5–10 min. Propagation of the various uncertainties for reliability analysis takes less than 3 min. When direct MCS is used

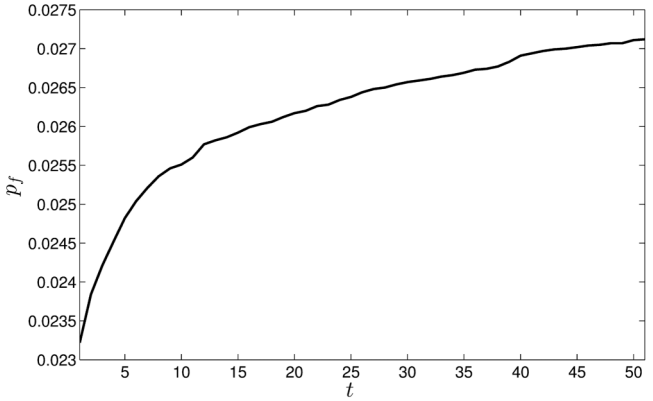

Fig. 11 Time-dependent failure probability for the curved beam (ignoring classification uncertainty).

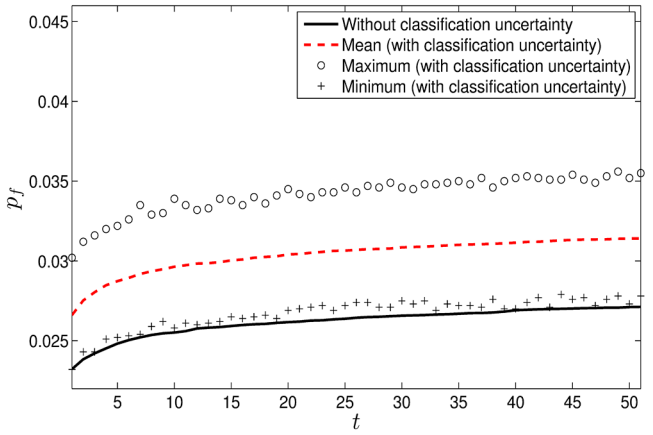

Fig. 12 Time-dependent failure probability with classification uncertainty.

(1×10^5 runs), it will take around 5 months to finish if a single desktop computer is used to run the simulations. When the proposed reliability analysis method is extended to realistic structures such as a hypersonic aircraft panel subjected to multiphysics loads, the computational cost of MCS will become much higher and unaffordable.

In this paper, the SVM is used as classifier for reliability analysis. The Artificial Neural Network (ANN) is also used in the literature for the modeling of disjoint failure boundaries [50]. However, Li et al. [51] have discussed that the selection of the topology structure and parameters, overfitting, and local minima makes ANN less effective than SVM in reliability analysis [52–54].

V. Conclusions

Snap-through buckling is an important failure mode to consider during the design of airframe structures subject to extreme environments. For problems with spatiotemporal variability, it is hard to identify a specific value of the critical buckling load, which is widely used in current buckling reliability analysis methods. To overcome this difficulty, this paper directly uses a classifier to perform buckling reliability analysis instead of relying on the critical buckling load. Based on the definition of the failure indicator function, a new snap-through buckling reliability analysis method is developed for problems under spatiotemporal variability and epistemic uncertainty.

There are mainly two challenges in buckling reliability analysis under spatiotemporal variability and epistemic uncertainty. The first challenge is how to represent the spatiotemporal variability based on available data and to quantify the epistemic uncertainty in this representation due to limited data. The second challenge is how to perform buckling reliability analysis by considering the spatiotemporal variability and epistemic uncertainty in characterizing spatiotemporal variability. To overcome the first challenge, this paper integrates singular value decomposition (SVD) with time-series modeling to effectively describe the spatiotemporal variability. The SVD is used to account for the variability and correlation over space, while an autoregressive moving average (ARMA) model is used to account for the variability and correlation over time. Bayesian calibration is employed to quantify the epistemic uncertainty in the SVD–ARMA model. A SVM-based classifier is developed for the time-dependent buckling reliability analysis. The SVM model is first trained for the various random quantities. After that, time-dependent reliability is analyzed using Monte Carlo simulation with the SVM model. The epistemic uncertainty introduced by limited training of the SVM model (due to computational resource constraints) is included to quantify the uncertainty in the reliability estimate. A curved beam with uncertain boundary condition, spatial variability in the material modulus, and spatiotemporal variability in the loading is used to demonstrate the proposed buckling reliability analysis method.

The SVM model is directly used to obtain the buckling failure indicator in this paper. No advanced sampling approach is used. Future work needs to explore adaptive sampling to optimize the number of training points for the SVM model, in order to maximize its accuracy and minimize its uncertainty. In addition, future work needs to incorporate verification and validation in the various steps of the proposed methodology. In this paper, the SVD–ARMA model is used to represent the spatial and temporal variability of loading. When practical laboratory data are used, several sources of uncertainty such as model uncertainty and observation uncertainty need to be considered. When there are too much data, directly performing SVD will create a high demand on the computer memory. In that case, a low-rank data compression method can be used to perform SVD and then model the coefficients in the ARMA models. Future work needs to account for the uncertainties of SVD–ARMA representation and investigate strategies to meet the computational demand in realistic problems. An important source of epistemic uncertainty, namely, physics model uncertainty, is not included in the methodology developed in this paper; this needs to be addressed in future work. Application of the developed method to more complicated air vehicle structures or components such as hypersonic panels also needs to be investigated in the future.

Acknowledgements

The research reported in this paper was supported by funding from the Air Force Office of Scientific Research (grant number FA9550-15-1-0018, under Technical Monitor David Stargel). The support is gratefully acknowledged.

References

[1] Abramovich, H., Weller, T., and Bisagni, C., "Buckling Behavior of Composite Laminated Stiffened Panels Under Combined Shear-Axial Compression," *Journal of Aircraft*, Vol. 45, No. 2, 2008, pp. 402–413. doi:10.2514/1.27635

[2] Miller, B. A., McNamara, J. J., Spottswood, S., and Culler, A., "The Impact of Flow Induced Loads on Snap-Through Behavior of Acoustically Excited, Thermally Buckled Panels," *Journal of Sound and Vibration*, Vol. 330, No. 23, 2011, pp. 5736–5752. doi:10.1016/j.jsv.2011.06.028

[3] Miskovish, R. S., Shah, P., and Spottswood, S. M., "Predicting Snap-through of a Thin-Walled Panel due to Thermal and Acoustic Loads," *SIMULIA Customer Conference*, Providence, RI, May 2010.

[4] Haftka, R. T., and Mallett, R. H., "Adaption of Koiter's Method to Finite Element Analysis of Snap-Through Buckling Behavior," *International Journal of Solids and Structures*, Vol. 7, No. 10, 1971, pp. 1427–1445. doi:10.1016/0020-7683(71)90055-2

[5] Virgin, L. N., *Vibration of Axially-Loaded Structures*, Cambridge Univ. Press, Cambridge, England, U.K., 2007, pp. 84–88.

[6] Wiebe, R., Virgin, L., Stanciulescu, I., and Spottswood, S., "On Snap-Through Buckling," *Collection of Technical Papers: AIAA/ASME/ASCE/AHS/ASC Structures, Structural Dynamics and Materials Conference*, AIAA Paper 2011-2083, 2011.

[7] Pi, Y. -L., Bradford, M., and Tin-Loi, F., "Nonlinear Analysis and Buckling of Elastically Supported Circular Shallow Arches," *International Journal of Solids and Structures*, Vol. 44, No. 7, 2007, pp. 2401–2425. doi:10.1016/j.ijsolstr.2006.07.011

[8] Przekop, A., and Rizzi, S. A., "Dynamic Snap-Through of Thin-Walled Structures by a Reduced-Order Method," *AIAA Journal*, Vol. 45, No. 10, 2007, pp. 2510–2519. doi:10.2514/1.26351

[9] Alibrandi, U., Impollonia, N., and Ricciardi, G., "Probabilistic Eigenvalue Buckling Analysis Solved Through the Ratio of Polynomial Response Surface," *Computer Methods in Applied Mechanics and Engineering*, Vol. 199, No. 9, 2010, pp. 450–464. doi:10.1016/j.cma.2009.08.015

[10] Papadopoulos, V., and Papadrakakis, M., "The Effect of Material and Thickness Variability on the Buckling Load of Shells with Random Initial Imperfections," *Computer Methods in Applied Mechanics and Engineering*, Vol. 194, No. 12, 2005, pp. 1405–1426. doi:10.1016/j.cma.2004.01.043

[11] Van de Lindt, J., and Pei, S., "Buckling Reliability of Deteriorating Steel Beam Ends," *Electronic Journal of Structural Engineering*, Vol. 6, No. 6, 2006, pp. 1–7.

[12] Choi, S.-K., Grandhi, R. V., and Canfield, R. A., "Structural Reliability Under Non-Gaussian Stochastic Behavior," *Computers and Structures*, Vol. 82, No. 13, 2004, pp. 1113–1121. doi:10.1016/j.compstruc.2004.03.015

[13] Hilburger, M. W., Nemeth, M. P., and Starnes, J. H., "Shell Buckling Design Criteria Based on Manufacturing Imperfection Signatures," *AIAA Journal*, Vol. 44, No. 3, 2006, pp. 654–663. doi:10.2514/1.5429

[14] Koiter, W., Elishakoff, I., Li, Y., and Starnes, J., "Buckling of an Axially Compressed Cylindrical Shell of Variable Thickness," *International Journal of Solids and Structures*, Vol. 31, No. 6, 1994, pp. 797–805. doi:10.1016/0020-7683(94)90078-7

[15] Starnes, J., Hilburger, M., and Nemeth, M., "The Effects of Initial Imperfections on the Buckling of Composite Cylindrical Shells," *Composite Structures: Theory and Practice*, edited by Grant, P., and Rousseau, C.ASTM International STP14529S, West Conshohocken, PA, 2001, pp. 529–550.

[16] Chryssanthopoulos, M., Giavotto, V., and Poggi, C., "Characterization of Manufacturing Effects for Buckling-Sensitive Composite Cylinders," *Composites Manufacturing*, Vol. 6, No. 2, 1995, pp. 93–101. doi:10.1016/0956-7143(95)99649-D

[17] Basudhar, A., and Missoum, S., "A Sampling-Based Approach for Probabilistic Design with Random Fields," *Computer Methods in Applied Mechanics and Engineering*, Vol. 198, No. 47, 2009, pp. 3647–3655. doi:10.1016/j.cma.2009.07.003

[18] Basudhar, A., and Missoum, S., "Reliability Assessment Using Probabilistic Support Vector Machines," *International Journal of Reliability and Safety*, Vol. 7, No. 2, 2013, pp. 156–173. doi:10.1504/IJRS.2013.056378

[19] Kennedy, M. C., and O'Hagan, A., "Bayesian Calibration of Computer Models," *Journal of the Royal Statistical Society: Series B (Statistical Methodology)*, Vol. 63, No. 3, 2001, pp. 425–464. doi:10.1111/rssb.2001.63.issue-3

[20] Kaplan, A., and Fung, Y., "A Nonlinear Theory of Bending and Buckling of Thin Elastic Shallow Spherical Shells," NACA TN-3212, Pasadena, CA, 1954.

[21] Fung, Y.-C., and Kaplan, A., *Buckling of Low Arches or Curved Beams of Small Curvature*, National Advisory Committee for Aeronautics TN-2840, Washington, D.C., 1952, Document ID: 19930083579.

[22] Elishakoff, I., Cai, G., and Starnes, J., "Non-Linear Buckling of a Column with Initial Imperfection via Stochastic and Non-Stochastic Convex Models," *International Journal of Non-Linear Mechanics*, Vol. 29, No. 1, 1994, pp. 71–82. doi:10.1016/0020-7462(94)90053-1

[23] Kogiso, N., Shao, S., and Murotsu, Y., "Effect of Correlation on Reliability-Based Design of Composite Plate for Buckling," *AIAA Journal*, Vol. 36, No. 9, 1998, pp. 1706–1713. doi:10.2514/2.576

[24] Elishakoff, I., Van Manen, S., and Arbocz, J., "First-Order Second-Moment Analysis of the Buckling of Shells with Random Imperfections," *AIAA Journal*, Vol. 25, No. 8, 1987, pp. 1113–1117. doi:10.2514/3.9751

[25] Sudret, B., and Der Kiureghian, A., "Comparison of Finite Element Reliability Methods," *Probabilistic Engineering Mechanics*, Vol. 17, No. 4, 2002, pp. 337–348. doi:10.1016/S0266-8920(02)00031-0

[26] Berkooz, G., Holmes, P., and Lumley, J. L., "The Proper Orthogonal Decomposition in the Analysis of Turbulent Flows," *Annual Review of Fluid Mechanics*, Vol. 25, No. 1, 1993, pp. 539–575. doi:10.1146/annurev.fl.25.010193.002543

[27] Willcox, K., and Peraire, J., "Balanced Model Reduction via the Proper Orthogonal Decomposition," *AIAA Journal*, Vol. 40, No. 11, 2002, pp. 2323–2330. doi:10.2514/2.1570

[28] Xi, Z., Youn, B. D., and Hu, C., "Random Field Characterization Considering Statistical Dependence for Probability Analysis and Design," *Journal of Mechanical Design*, Vol. 132, No. 10, 2010, Paper 101008. doi:10.1115/1.4002293

[29] Chatterjee, A., "An Introduction to the Proper Orthogonal Decomposition," *Current Science*, Vol. 78, No. 7, 2000, pp. 808–817.

[30] Nelson, C. R., and Plosser, C. R., "Trends and Random Walks in Macroeconmic Time Series: Some Evidence and Implications," *Journal of Monetary Economics*, Vol. 10, No. 2, 1982, pp. 139–162. doi:10.1016/0304-3932(82)90012-5

[31] Kothari, S. P., and Shanken, J., "Book-to-Market, Dividend Yield, and Expected Market Returns: A Time-Series Analysis," *Journal of Financial Economics*, Vol. 44, No. 2, 1997, pp. 169–203. doi:10.1016/S0304-405X(97)00002-0

[32] Cheong, B., Palmer, R., and Xue, M., "A Time Series Weather Radar Simulator Based on High-Resolution Atmospheric Models," *Journal of Atmospheric and Oceanic Technology*, Vol. 25, No. 2, 2008, pp. 230–243. doi:10.1175/2007JTECHA923.1

[33] Schneider, T., and Neumaier, A., "Algorithm 808: ARfit—A Matlab Package for the Estimation of Parameters and Eigenmodes of Multivariate Autoregressive Models," *ACM Transactions on Mathematical Software*, Vol. 27, No. 1, 2001, pp. 58–65. doi:10.1145/382043.382316

[34] Shumway, R. H., and Stoffer, D. S., *Time Series Analysis and its Applications*, Springer–Verlag, New York, 2009, pp. 121–127.

[35] Huang, S.-J., and Shih, K.-R., "Short-Term Load Forecasting via ARMA Model Identification Including Non-Gaussian Process Considerations," *IEEE Transactions on Power Systems*, Vol. 18, No. 2, 2003, pp. 673–679. doi:10.1109/TPWRS.2003.811010

[36] Singh, N., "Forecasting Time-Dependent Failure Rates of Systems Operating in Series and/or in Parallel," *Microelectronics Reliability*, Vol. 34, No. 3, 1994, pp. 391–403. doi:10.1016/0026-2714(94)90080-9

[37] Forsberg, F., "On the Usefulness of Singular Value Decomposition-ARMA Models in Doppler Ultrasound," *IEEE Transactions on Ultrasonics, Ferroelectrics, and Frequency Control*, Vol. 38, No. 5, 1991, pp. 418–428. doi:10.1109/58.84286

[38] Jibia, A. U., and Salami, M.-J. E., "Parameter Estimation of Transient Multiexponential Signals Using SVD-ARMA and Multiparameter Deconvolution Techniques," *International Journal of Computer Theory and Engineering*, Vol. 4, No. 5, 2012, pp. 751–757. doi:10.7763/IJCTE.2012.V4.571

[39] Green, P. J., "Reversible Jump Markov Chain Monte Carlo Computation and Bayesian Model Determination," *Biometrika*, Vol. 82, No. 4, 1995, pp. 711–732. doi:10.1093/biomet/82.4.711

[40] Uturbey, W., "Identification of ARMA Models by Bayesian Methods Applied to Streamflow Data," *IEEE International Conference on Probabilistic Methods Applied to Power Systems (PMAPS)*, Inst. of Electrical and Electronics Engineers, Stockholm, Sweden, 2006, pp. 1–7.

[41] Basudhar, A., and Missoum, S., "Adaptive Explicit Decision Functions for Probabilistic Design and Optimization Using Support Vector Machines," *Computers and Structures*, Vol. 86, No. 19, 2008, pp. 1904–1917. doi:10.1016/j.compstruc.2008.02.008

[42] Hu, Z., and Du, X., "Time-Dependent Reliability Analysis with Joint Upcrossing Rates," *Structural and Multidisciplinary Optimization*, Vol. 48, No. 5, 2013, pp. 893–907. doi:10.1007/s00158-013-0937-2

[43] Hu, Z., and Du, X., "A Sampling Approach to Extreme Value Distribution for Time-Dependent Reliability Analysis," *Journal of Mechanical Design*, Vol. 135, No. 7, 2013, Paper 071003.

[44] Suykens, J. A., and Vandewalle, J., "Least Squares Support Vector Machine Classifiers," *Neural Processing Letters*, Vol. 9, No. 3, 1999, pp. 293–300. doi:10.1023/A:1018628609742

[45] Zou, T., Mourelatos, Z. P., Mahadevan, S., and Tu, J., "An Indicator Response Surface Method for Simulation-Based Reliability Analysis," *Journal of Mechanical Design*, Vol. 130, No. 7, 2008, Paper 071401. doi:10.1115/1.2918901

[46] Jiang, P., Missoum, S., and Chen, Z., "Optimal SVM Parameter Selection for Non-Separable and Unbalanced Datasets," *Structural and Multidisciplinary Optimization*, Vol. 50, No. 4, 2014, pp. 523–535. doi:10.1007/s00158-014-1105-z

[47] Huang, S., Mahadevan, S., and Rebba, R., "Collocation-Based Stochastic Finite Element Analysis for Random Field Problems," *Probabilistic Engineering Mechanics*, Vol. 22, No. 2, 2007, pp. 194–205. doi:10.1016/j.probengmech.2006.11.004

[48] Sankararaman, S., and Mahadevan, S., "Separating the Contributions of Variability and Parameter Uncertainty in Probability Distributions," *Reliability Engineering and System Safety*, Vol. 112, No. 112, April 2013, pp. 187–199. doi:10.1016/j.ress.2012.11.024

[49] Nannapaneni, S., and Mahadevan, S., "Model and Data Uncertainty Effects on Reliability Estimation," *17th AIAA Non-Deterministic Approaches Conference*, AIAA Paper 2015-1813, 2015.

[50] Schueremans, L., and Van Gemert, D., "Benefit of Splines and Neural Networks in Simulation Based Structural Reliability Analysis," *Structural Safety*, Vol. 27, No. 3, 2005, pp. 246–261. doi:10.1016/j.strusafe.2004.11.001

[51] Li, H., Lü, Z., and Yue, Z., "Support Vector Machine for Structural Reliability Analysis," *Applied Mathematics and Mechanics*, Vol. 27, No. 10, 2006, pp. 1295–1303. doi:10.1007/s10483-006-1001-z

[52] Lacaze, S., and Missoum, S., "A Generalized "Max-Min" Sample for Surrogate Update," *Structural and Multidisciplinary Optimization*, Vol. 49, No. 4, 2014, pp. 683–687. doi:10.1007/s00158-013-1011-9

[53] Basudhar, A., and Missoum, S., "An Improved Adaptive Sampling Scheme for the Construction of Explicit Boundaries," *Structural and Multidisciplinary Optimization*, Vol. 42, No. 4, 2010, pp. 517–529. doi:10.1007/s00158-010-0511-0

[54] Litvinenko, A., Matthies, H. G., and El-Moselhy, T. A., "Sampling and Low-Rank Tensor Approximation of the Response Surface," *Monte Carlo and Quasi-Monte Carlo Methods 2012*, Springer–Verlag, Berlin, 2013, pp. 535–551.

P. Weaver
Associate Editor